Numerical Modeling of Breaking Wave Induced Seawall Scour

Nadeem Ahmad[a,1], Hans Bihs[a], Dag Myrhaug[b], Arun Kamath[a], Øivind A. Arntsen[a]

[a] *Department of Civil and Transport Engineering, Norwegian University of Science and Technology, 7491 Trondheim, Norway.*
[b] *Department of Marine Technology, Norwegian University of Science and Technology, Trondheim, 7491, Norway*

Abstract

Scour is recognised as one of the major causes of seawall failure. This paper presents numerical modelling of seawall scour due to wave impact on a vertical seawall. The modelling of waves hydrodynamics is based on the solution of the Reynolds-Averaged Navier-Stokes equations with the k-ω model. Fifth-order Stokes waves are generated in a numerical wave tank (NWT) using the relaxation method. The free surface under the breaking wave is captured with the level set method. The wave field is coupled with a sediment transport algorithm to simulate seawall scour. The model is validated for an accurate wave field and the seawall scour due to the wave impact. The accuracy of the simulations is assured by comparing the numerical results with the theory and the experimental observations. The numerical results give insight into the seawall scour process through different stages. The results show that the seawall scour is governed by the breaking wave impact on the seawall. The development of the standing wave due to the reflected wave energy from the seawall leads to further sediment transport seawards. Finally, the model is used to simulate seawall scour for different scenarios of seawall locations, incident wave height and seabed slope. The study examines the wave impact on the seawall toe and resulting scour. The maximum seawall scour is observed when the seawall is located at the intersection point of the still water depth and the bed slope. A displacement of the seawall from the intersection point leads to a decrease in the wave impact. The surf similarity parameter ξ_0 is recognised as an important factor affecting the seawall scour.

Keywords: Coastal erosion, Wave impact, Seawall scour, Standing waves, Free surface, CFD.

[1] Corresponding Author, Email: nadeem.ahmad@ntnu.no, Ph: (+47) 93 97 91 60, Fax: (+47) 73 59 70 21

1. Introduction

Seawalls are common structures in several coastal regions. They are built along the coastline to prevent erosion during severe storm conditions. It is expected that seawalls have to deal with changing impact scenarios due to climate change, such as sea level rise, higher waves approaching the seawall, changes in bed profile and the extreme storms [1]. These changes lead to increased wave impact on the seawalls. As vertical seawalls are considered to be relatively ineffective for wave energy dissipation, the wave impact on the seawall leads to higher seawall scour which is considered to be the major cause of the seawall failure [2]. Therefore, while seawalls are an effective protection measure against erosion of the coastline, seawall scour needs to be analysed in order to guarantee their structural stability. The process of seawall scour is described as follows: when a wave impacts the seawall, the water runs up along the seawall and returns towards the still water level in the form of a vertical jet. This results in higher scour at the seawall toe. After the impact, the water is reflected seawards which creates turbulence, making the region near to the seawall more susceptible to scour.

Existing literature has investigated seawall scour based on field and experimental investigations. Dean [3] measured the influence of the seawall on the coastline. It was found that the presence of the seawall leads to steepening of the seabed profile and increasing scour at the seawall toe. Hughes and Fowler [4] and Fowler [5] presented the scaling factor appropriate for seawall scour modelling in the laboratory. The scour profiles on slopes were reproduced to validate a set of modelling criteria and constraints for the prediction of scour under different wave conditions. Kamphuis et al. [6] discussed a three-dimensional experimental investigation of seawall scour together with long-shore sediment transport. It was reported that the longshore sediment transport rate in front of the seawall decreases with the seawall scour depth. Kraus and Smith [7] discussed sediment transport measurements using a large wave tank. It was revealed that the presence of a seawall mostly changes the immediate beach profile. However, the major part of the seabed profile remained unaffected. In a study based on the collection of experimental data of seawall scour, Kraus and McDougal [2] reported that the maximum scour depth at the seawall toe is determined to be $S/H_0 \leq 1.0$, where S is the maximum scour depth at the seawall toe and H_0 is the incident deepwater wave height. Amongst the recent experimental investigations, Sumer and Fredsøe [8] performed a two-dimensional scour analysis at a vertical breakwater placed on a flat seabed. The breakwater was exposed to regular and irregular waves. It was found that the scour and the deposition pattern develops in the form of alternating scour and deposition. In addition, the scour depth under irregular waves was ob-

served to be lower compared to regular waves. Sutherland et al. [9] investigated seawall scour for vertical and inclined seawalls placed on a sloping seabed. It was found that the maximum scour depth depends on the relative water depth at the seawall toe and the surf similarity parameter ξ_0. In addition, the study showed that the maximum scour depth is insensitive to the seawall slope; an inclined seawall reproduced similar scour depths as a vertical seawall. Tsai et al. [10] studied seawall scour under breaking waves and demonstrated that the maximum scour depth at the seawall toe decreases with an increase in the water depth at the seawall toe.

The numerical modelling of cross-shore sediment transport under breaking waves impact is a challenging task, and only limited progress has been made in this area so far. Dally and Dean [11] investigated the evolution of the seabed profile using a simplified analytical model. The study discussed the suspended sediment transport in onshore-offshore direction and the change in seabed profile with regards to the still water depth. Roelvink and Stive [12] examined the cross-shore flow mechanisms and the associated changes in seabed profile under random waves. The return flow and the additional bed shear stress due to the wave breaking on a sloping bed were considered a governing factor for the change in seabed profile.

McDougal et al. [13] were the first to attempt numerical modelling of the cross-shore profile with a seawall. The study was performed using a simple mathematical model based on empirical equations of the waves and sediment transport. The effect of the reflected wave on the cross-shore sediment transport was analysed. The investigation revealed that the reflected waves from the seawall strongly affect the immediate seabed profile. Gislason et al. [14] investigated the formation of standing waves and resulting scour at a breakwater placed on a flat bed by solving the Reynolds-Averaged Navier-Stokes (RANS) equations with a sediment transport model. The study investigated the formation of standing waves and the resulting scour agreed well with experiments by Sumer and Fredsøe [8]. It was observed that S/H_0 decreases with increasing water depth. However, the influence of the sloping seabed and wave breaking were not accounted for in the scour calculations. Non-breaking waves were computed using the kinematic boundary condition based on the free surface volume flux. Myrhaug and Ong [15] presented a stochastic method by which the random wave-induced scour depth at the trunk section of vertical-wall and rubble-mound breakwaters can be derived. The formulas for regular wave-induced scour depth provided by Xie [16] and Sumer and Fredsøe [8] were used to derive the random wave-induced scour depth by describing the waves as a stationary Gaussian narrow-band random process. Zou et al. [17] attempted to model the same case from Sumer and Fredsøe [8] by employing the volume-of-fluid (VOF) method to capture the breaking waves. In a recent study, Ahmad et al.

[18] investigated the numerical modelling of an Arctic Bluff with a sloping bed. RANS equations coupled with a sediment transport model was used to simulate the scour process. The level-set-method (LSM) was used to capture the free surface including breaking waves. The study demonstrated the hydrodynamics of the waves breaking and the resulting scour at a vertical bluff.

The primary objective of this paper is to investigate seawall scour. The open-source CFD model REEF3D, which has already been validated for breaking waves [19, 20], is applied for a detailed investigation of the scouring process. The study focuses on seawall scour due to wave impact on a vertical seawall and the formation of standing waves, which increases the scour in the region near the seawall. The wave-impact and the resulting seawall scour depend on the kinematic properties of breaking waves during the impingement on the vertical seawall. Several scenarios with different seawall locations, wave height, and seabed slopes are simulated and the effect of those changes is analyzed in detail. The numerical results are compared with the available experimental data from Hughes and Fowler [4] and Kraus and McDougal [2].

2. Numerical model description

The numerical modelling is performed with the open-source CFD model REEF3D [21, 22]. The model has been successfully applied for wave-induced scour in coastal environments, such as the wave-induced scour around vertical piles [23, 24], modelling of breaking waves [19, 20] and resulting scour [18]. The modelling of sediment transport processes involves different modules, such as the generation of waves, free surface capturing, bed load and suspended transport, and the calculation of morphological changes. A description of the modules is given below.

2.1. Hydrodynamic model

The flow field in a numerical wave tank (NWT) is based on the solution of the incompressible Reynolds-Averaged Navier-Stokes (RANS) equations and the continuity equation:

$$\frac{\partial u_i}{\partial x_i} = 0 \tag{1}$$

$$\frac{\partial u_i}{\partial t} + u_j \frac{\partial u_i}{\partial x_j} = -\frac{1}{\rho}\frac{\partial p}{\partial x_i} + \frac{\partial}{\partial x_j}\left[(\nu + \nu_t)\left(\frac{\partial u_i}{\partial x_j} + \frac{\partial u_j}{\partial x_i}\right)\right] + g_i \tag{2}$$

where u_i is the fluid velocity, p is the pressure, ρ is the fluid density, ν is the fluid kinematic viscosity, ν_t is the eddy viscosity and g is the gravitational acceleration. The value of the eddy-viscosity is obtained using the two-equation k-ω model from Wilcox [25].

2.2. Free surface model

The dynamic free surface is modelled with the level set method [26]. With two phase approach the interface is determined implicitly using a continuous signed distance function $\phi(\vec{x},t)$. The negative and positive values of the level set function $\phi(\vec{x},t)$ distinguish the air and water phase, respectively. The zero level set of $\phi(\vec{x},t)$ represents the free surface as:

$$\phi(\vec{x},t)\begin{cases} > 0 & if\ \vec{x}\ is\ in\ the\ water \\ = 0 & if\ \vec{x}\ is\ at\ the\ free\ surface \\ < 0 & if\ \vec{x}\ is\ in\ the\ air \end{cases} \tag{3}$$

The evolution of the free surface over time is calculated with a transport equation. The fluid velocity u_j obtained from the RANS equations is used to convect the level set function $\phi(\vec{x},t)$ as follows:

$$\frac{\partial \phi}{\partial t} + u_j \frac{\partial \phi}{\partial x_j} = 0 \tag{4}$$

As the free surface evolves, the level set function $\phi(\vec{x},t)$ loses its signed distance property. Therefore, the solution is reinitialised each time step to maintain the signed distance property and the mass conservation [27]. The partial differential equation (PDE) approach [28] is used for the reinitialisation as follows:

$$\frac{\partial \phi}{\partial \tau} + S\left(\phi\right)\left(\left|\frac{\partial \phi}{\partial x_j}\right| - 1\right) = 0 \tag{5}$$

where $S\left(\phi\right)$ is the smoothed signed distance function [27].

2.3. Sediment transport model

In this section, the numerical approach for the sediment transport calculations is given. The model has already been described in detail by Ahmad et al. [23], and an overview is presented here. The calculation of the bed load transport is based on the formulation proposed by van Rijn [29]. It calculates the incipient motion of the sediment particles based on the bed shear stress at the sediment bed. When the bed shear stress is larger than the critical bed shear stress, it leads to sediment particles rolling and sliding in form of the bed load. The bed load is calculated as [29]:

$$\frac{q_{b,i}}{d_{50}^{1.5}\sqrt{(s-1)g}} = 0.053\ \frac{T^{2.1}}{D_*^{0.3}} \tag{6}$$

Here, $T = \frac{\tau - \tau_{cr}}{\tau_{cr}}$ is the transport stage parameter and $D_* = d_{50}\left[\frac{(s-1)g}{\nu^2}\right]^{1/3}$ is the particle parameter. The transport stage parameter represents the critical condition of the initiation of sediment motion. The particle parameter is a non-dimensional term obtained by removing the shear velocity from the particle mobility parameter and particle Reynolds number [29]. The other terms in the formulations are defined as follows: $\tau = \rho u_*^2$ is the bed shear stress, $u_* = u\ \kappa / ln\ (\frac{30z}{k_s})$ is the shear velocity, u is the water velocity at a height z above the bed, $\kappa = 0.4$ is the von Karman constant, $k_s = 3d_{50}$ is the equivalent sand roughness and d_{50} is the median grain size, $s = \rho_s/\rho$ is the specific density, ρ_s is the sediment density and ρ is the water density.

The general approach to calculate the critical bed shear stress (τ_0) is to use the Shields graph which is based on experiments without accounting for the effect of a sloping bed. The bed profile of a scour hole consists of longitudinal and transversal sloping beds. Therefore, the modified critical bed shear stress $\tau_{cr} = r\ \tau_0$ is considered. The term r is the modification factor which includes the effect of the sloping bed and is calculated as suggested by Dey [30] as:

$$\begin{aligned} r = \frac{1}{\big(1 - \eta \tan\varphi\big)\tan\varphi} \Big\{ & -\big(\sin\theta + \eta \tan^2\varphi \sqrt{\cos^2\theta - \sin^2\alpha}\big) \\ & + \big[\big(\sin\theta + \eta \tan^2\varphi \sqrt{\cos^2\theta - \sin^2\alpha}\ \big)^2 \\ & + \big(1 - \eta^2 \tan^2\varphi\big)\big(\cos^2\theta \tan^2\varphi - \sin^2\alpha \tan^2\varphi - \sin^2\theta - \sin^2\alpha\big)\big]^{0.5} \Big\} \end{aligned} \tag{7}$$

where θ is the longitudinal bed slope, α is the transversal bed slope, φ is the angle of repose and η is the ratio of the drag force to the inertia force. The formulation for the reduction factor r results in a decrease in the critical bed shear stress on a downhill slope and an increase for an uphill slope [31].

The model for the suspended load transport corresponds to that of van Rijn [32]. It accounts for the sediments in the water column away from the bed. A convection-diffusion equation is solved to obtain the suspended load concentration. The numerical treatment of the equation is performed in a similar way as for the momentum equations.

$$\frac{\partial c}{\partial t} + u_j \frac{\partial c}{\partial x_j} + w_s \frac{\partial c}{\partial z} = \frac{\partial}{\partial x_j}\left(\Gamma \frac{\partial c}{\partial x_j}\right) \tag{8}$$

where c is the suspended load concentration, w_s is the fall velocity of the sediment particles and Γ is the sediment mixing coefficient. The value of Γ is considered equal to the eddy-viscosity

[33]. The boundary conditions to solve the convection-diffusion equation assume a zero sediment concentration at the free surface. The suspended load concentration at the bottom is calculated using the van Rijn [32] formula: $c_b = 0.015\frac{d_{50}}{a}\left(\frac{T^{1.5}}{D_*^{0.3}}\right)$, where a is the reference level for the suspended load and is equal to the equivalent-roughness height as $k_s = 3d_{50}$. The suspended load concentration close to the bed is interpolated with the Rouse equation [34] as:

$$c(z) = c_b\left(\frac{h-z}{z}\frac{a}{h-a}\right)^z \tag{9}$$

where z is the distance from the nearest grid point to the seabed as suggested by Olsen [35].

2.4. Morphological model

The transient evolution of the seabed profile is obtained with Exner's formula. The formula is based on the local mass balance of sediments. It involves a non-linear propagation of the bed-level deformation in the direction of the sediment transport and the spacial variation of the sediment fluxes between the bed load and suspended load. The equation becomes:

$$\frac{\partial z_b}{\partial t} + \frac{1}{(1-n)}\left[\ \frac{\partial q_{b,x}}{\partial x}\ \right] + (E-D) = 0 \tag{10}$$

Here, z_b is the bed-level, $q_{b,x}$ is the bed-load in the x-direction and $n = 0.40$ is the sediment porosity. The term $(E - D)$ defines the net sediment movement between the bed load and suspended load. The sediment bed and the fluid is distinguished through the zero level set and thus movable bed is implicitly defined through a level set function. No remeshing close to the seabed is needed under sediment transport. The failure of scour hole slopes is incorporated into the model. The sediment begins to slide when the bed slope exceeds the angle of repose (φ). This feature is accounted for with a sand slide algorithm [36, 37].

2.5. Numerical solver and schemes

The partial differential equations for the flow and turbulence are solved using advanced finite difference methods. The convective terms of the RANS equations, the level set function and the suspended load equations are discretised with the fifth-order accurate Weighted Essential Non-Oscillatory (WENO) scheme [38]. The time treatment of the governing equations is dealt with a third-order TVD Runge-Kutta time scheme [39]. The time step for the transient flow is determined using adaptive time stepping. The size of the time step is controlled with the Courant-Friederichs-Lewy (CFL) number [40]. The pressure is treated with the projection

method [41]. The BiCGStab [42] solver from the high-performance solver package HYPRE with the semi-coarsening multi-grid preconditioner PFMG [43] is employed to solve the Poisson equation for the pressure.

2.6. Generation of waves and boundary conditions in NWT

The wave generation in the NWT is managed with the relaxation method [44]. Fifth-order Stokes waves are generated by prescribing the wave elevation η and the flow velocities in the relaxation zone. The computational values are transformed to the analytical values of the incident wave along the relaxation zone using the relaxation function $\Gamma(x)$ as follows:

$$\Gamma(x) = 1 - \frac{exp(x^{3.5}) - 1}{exp(1) - 1} \tag{11}$$

and is applied inside the relaxation domain as follows:

$$\begin{aligned} (u) &= \Gamma(x) u_{computed} + [1 - \Gamma(x)] u_{target} \\ \phi &= \Gamma(x) \phi_{computed} + [1 - \Gamma(x)] \phi_{target} \end{aligned} \tag{12}$$

Here, x is the normalized length scale which varies from 0 to 1. The bottom of the NWT is considered as a wall. The sides and the top of the NWT are treated as symmetry planes. The boundary of the solid seawall and the concrete revetment are defined with an immersed boundary method using the local directional ghost cell approach [45]. The sediment seabed is assumed to be hydraulically rough with a roughness height of $k_s = 3d_{50}$. An overview over the computational domain and the boundary conditions can be found in Fig. 1(a).

3. Results

3.1. Numerical setup

The computational setup for the model validation follows the layout of Hughes and Fowler [4]. Their experimental tests were conducted in a 100 m long, 1.83 m wide, and 1.83 m deep wave flume. The numerical simulations are performed in a 2D NWT. The length of the wave generation zone is 10.0 m, followed by a 28.71 m flat bed and a sloping bed with the seawall. The seabed slope is m = 1:4. The sloping seabed is made of a sand berm with a horizontal berm width of 1.46 m placed on top of the concrete revetment. Regular waves are used to investigate the seawall scour. The incident wave height, still water depth and the wave period of the approaching wave to the sand berm are H_0 = 0.20 m, h = 0.67 m and T = 2.2 s,

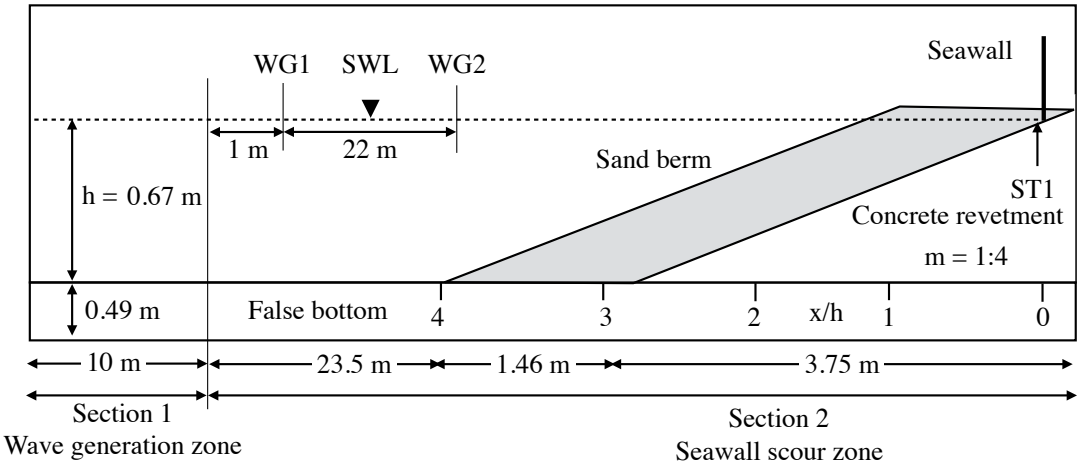

(a)

Figure 1: The numerical setup used for the modelling of seawall scour. The term ST1 refers to a location at the seawall toe. The figure is not to scale. Source of the experimental data: Hughes and Fowler [4]

respectively. The wavelength and the surf similarity parameter are calculated to be $\lambda_0 = 5.5$ m and $\xi_0 = m/\sqrt{H_0/\lambda_0} = 1.31$ (>0.55), respectively. This indicates plunging for the breaking waves on the slope. The bed material used for the sand berm consists of sand with a median particle diameter $d_{50} = 0.13$ mm. The sediment density is $\rho_s = 2650$ kg/m^3. The critical Shields parameter for the bed material is $\theta_c = 0.047$. The seawall is placed at the intersection between the concrete revetment and the still water level. Based on the incident wave characteristics, fifth-order Stokes wave theory is chosen for the wave generation in the NWT.

3.2. Grid convergence study

In order to test the quality of the waves generated in the NWT, a grid convergence study is performed. The waves are generated and propagated over the sloping sand berm without the seawall [4]. The simulations are run without sediment transport calculation. For all simulations, the CFL-number is 0.1, as was shown in Bihs et al. [21]. The accuracy of the simulated waves is evaluated by comparing the simulated wave elevations to wave theory and as measured in the experiment [4]. The wave surface elevations are measured at two wave gauges. The first wave gauge WG1 is located 1.0 m away from the wave generation zone. The purpose is to ensure that there is no influence of the reflected waves from the sloping bed on the wave generation zone. The wave elevations are compared with fifth-order Stokes wave theory. The second wave gauge WG2 is located 0.5 m before the sand berm and the wave elevations at this location are compared with the experimental data. All simulations for hydrodynamic validations are run

No	dx	x/h	m	$h(m)$	$T(s)$	H_0 (m)	λ_0 (m)	H_0/λ_0	ξ_0	S/h
Model validation										
A1	0.40	-	1:4	0.67	2.2	0.20	5.5	0.036	1.31	-
A2	0.30	-	1:4	0.67	2.2	0.20	5.5	0.036	1.31	-
A3	0.20	-	1:4	0.67	2.2	0.20	5.5	0.036	1.31	-
A4	0.10	-	1:4	0.67	2.2	0.20	5.5	0.036	1.31	-

Table 1: A summary of simulations run for different grid convergence scenarios

for 50 waves. Four grid sizes of $dx = 0.03$ m, 0.02 m, and 0.01 m are tested. Details of the simulations run for the grid convergence study are given in Table 1.

Fig. 2(a) shows the wave field in a 2D NWT with a sloping seabed. The breaking waves are seen at $x = 36$ m. Figs. 2(b-e) show the simulated wave surface elevations measured at WG1. The quality of the wave is seen to be improving with a decreasing grid size dx. Fig. 2(f) shows the accuracy of the simulated waves corresponding to fifth-order Stokes wave theory. The accuracy of the simulated waves is calculated in terms of the error of the wave crests $\delta_{cr} = 100 * (\eta_{max,s} - \eta_{max,t})/H_0$, the wave troughs $\delta_{tr} = 100 * (\eta_{min,s} - \eta_{min,t})/H_0$ and the wave phase $\delta_{ph} = 100 * (t_{p,s} - t_{p,t})/T$, corresponding to fifth-order Stokes wave theory. Here, $\eta_{max,s}$ is the simulated wave crest, $\eta_{max,t}$ is the theoretical wave crest, $\eta_{min,s}$ is the simulated wave trough, $\eta_{max,t}$ is the theoretical wave trough, $t_{p,s}$ is the simulated peak period and $t_{p,s}$ is the theoretical peak period. For the coarse grid $dx = 0.04$ m, the simulated troughs and crests of the wave show an error range between 5 - 7% which converges to almost zero when the grid size is reduced to $dx = 0.01$ m. The simulated wave phase shows a relatively close fit with the wave theory, even for the coarse grid. The error in the wave phase decreases from 3% to 1% when the grid size is reduced to $dx = 0.01$ m. The quality of the simulated wave is considered sufficient at $dx = 0.01$ m showing no influence of reflections in the wave generation zone. To ensure the quality of the incident waves approaching the sloping seabed, the wave elevation measured at the wave gauge WG2 are compared with the experimental measurements for $dx = 0.01$. The simulated wave troughs depict an adequate match with the experimental data [4]. However, the simulated wave crests are slightly lower at $t/T = 35$. This is likely due to reflections in the experimental setup, which are prevented in the NWT with the relaxation method. The solution is assumed to converge at $dx = 0.01$ m. The model has been validated for breaking waves and further details can be found in Alagan Chella et al. [19, 20].

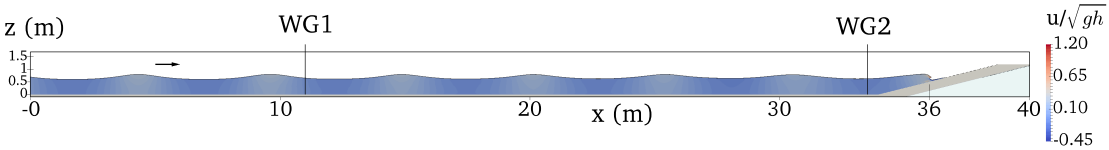

(a) The instantaneous free surface profile of the simulated plunging wave in a complete NWT with the sand berm as well the positions of the wave gauges

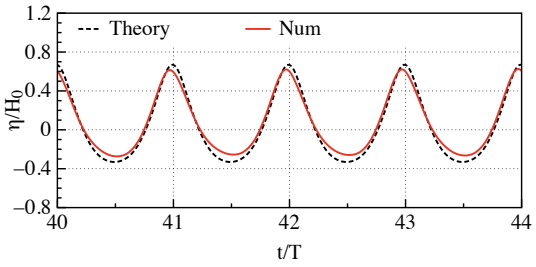

(b) dx = 0.04 m, location: WG1

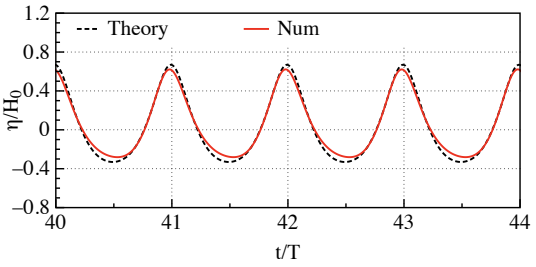

(c) dx = 0.03 m, location: WG1

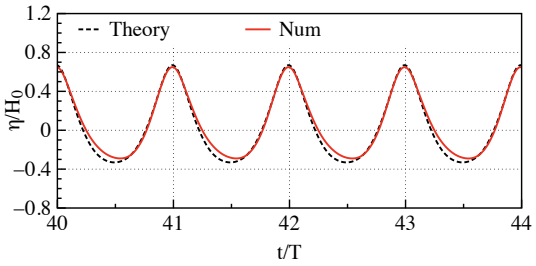

(d) dx = 0.02 m, location: WG1

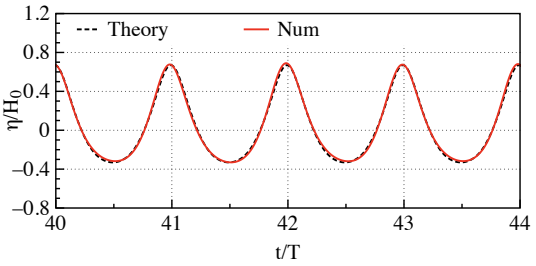

(e) dx = 0.01 m, location: WG1

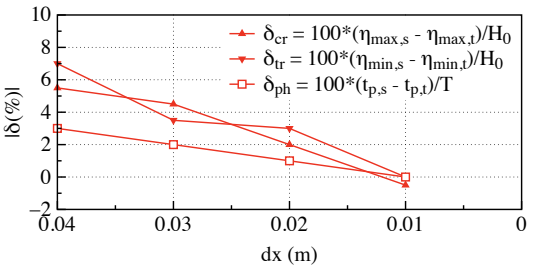

(f) The deviation of the simulated wave corresponding to the fifth-order wave theory

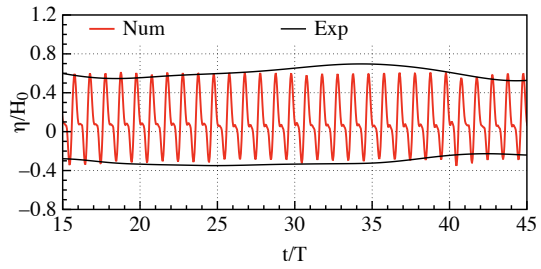

(g) The simulated wave elevations. The grid size dx = 0.01 m, wave gauge location: WG2

Figure 2: Illustration of the simulated wave profile in the grid convergence study. The bed slope is m = 1:4, The wave gauge WG1 is located 1.0 m away from wave generation zone and WG2 is placed 0.5 m before the sloping bed. Incident wave characteristics: H_0 = 0.20 m, T = 2.2 s, λ_0 = 5.5 m, H_0/λ_0 = 0.036 and the surf similarity parameter is $\xi_0 = m/\sqrt{H_0/\lambda_0}$ = 1.31. The red solid line depicts the numerical results, the black dashed line is fifth-order Stokes wave theory and the black solid line is the experiment [4]

3.3. Scour due to wave impact on a vertical seawall

This section describes the seawall scour due to the wave impact by enabling the sediment transport model for scour calculations. The simulation is performed with a seawall installed at the intersection of the concrete revetment and the still water level as in the experiment [4]. The results highlight the complex wave hydrodynamics on a sloping bed such as the wave breaking, the interaction of the reflected wave with the wave breaking process, followed by the development of a standing wave and the resulting scouring process. The changes in seabed elevation are associated with the flow hydrodynamics but take place much slower compared to the flow hydrodynamics. This implies that a morphological time step larger than the hydrodynamic time step can be used for the scour calculations. This is achieved by increasing the sediment time step with a decoupling factor $DF = \Delta t_m/\Delta t$, where Δt_m is the time step for the morphological model and Δt is the time step for the hydrodynamic model. The decoupling factor for this study is $DF = 25$. Details of the method and the procedure to select the decoupling factor can be found in Ahmad et al. [23]. The model is first run for the wave hydrodynamics for 5 waves and then the morphological calculations are performed for $t_m/T = 1650$ (66 regular wave periods).

Fig. 3 shows the scour due to breaking waves impact on the seawall. The results are shown in terms of velocity contours and velocity vectors with streamlines at different stages of the scour evolution close to the seawall. The process is described with regard to the interaction of the incident waves and the reflected wavefront from the seawall. Fig. 3(a) shows the situation at $t_m/T = 10$, when an incident wavefront is breaking at $x/h = 2.0$ and a reflected wavefront from the seawall at $x/h = 0.5$ is moving seawards (see Fig. 1(a) for the location in the NWT). In Fig. 3(b), the incident wavefront is past the initial wave breaking phase and the water is being pushed upwards in the form of a swash. The free surface level of the swash is seen to be $z/h = 1.3$ with the velocities ranging between $u/\sqrt{gh} = 0.80$ and 1.20. The velocities close to the bottom are seen to in the range between $u/\sqrt{gh} = 0.0$ and 0.30. At the same time, the reflected wave from the seawall is located at $x/h = 1.0$. The free surface level of the reflected wavefront is seen to be $z/h = 1.2$.

Fig. 3(c) depicts the reflected wavefront with a relatively low free surface with high velocities moving towards the swash with a higher free surface level and low velocities close to the bed. This results in a visible vortex structure at $x/h = 1.5$, which creates more turbulence. Subsequently, the sediments are eroded which makes this region more susceptible to scour. Fig. 3(d) shows the situation at $t_m/T = 10.7$ when a return flow mobilises the stirred-up sediments seawards. The swash is moving in seawall direction, runs up the seawall and plunges back in the form of

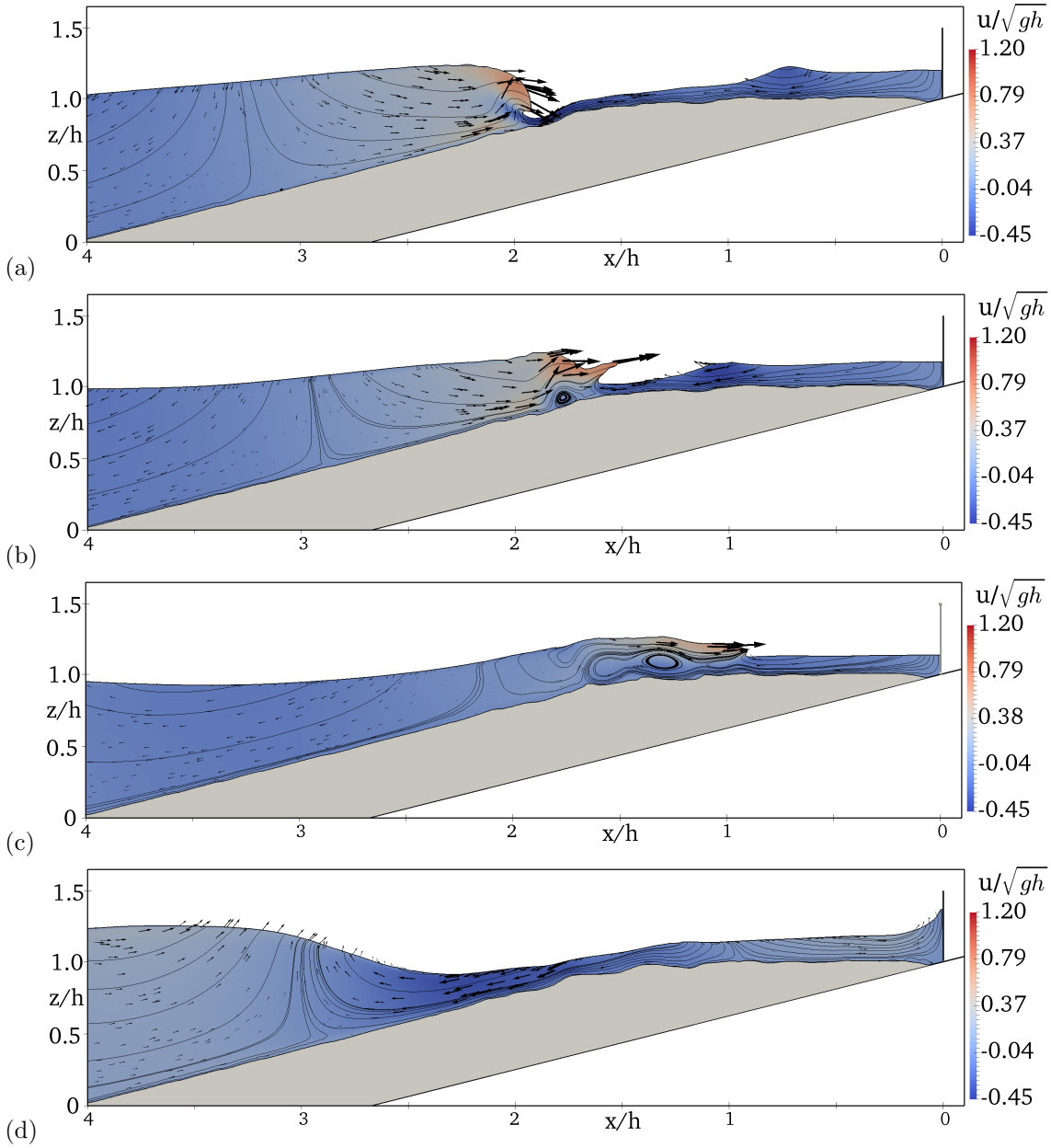

Figure 3: Illustration of scouring process due to the wave breaking and impact on the seawall during the initial stage at time interval (a) $t_m/T = 10$, (b) $t_m/T = 10.1$, (c) $t_m/T = 10.3$, (d) $t_m/T = 10.7$

the vertical jet towards the seawall toe which results in higher scour.

Figs. 4(a-c) show an intermediate stage of the scouring process after $t_m/T = 800$. The results show a removal of sediments from the seawall toe up to $x/h = 0.25$ from the seawall and a visible scour at $x/h = 1.5$. At this stage, two major changes in the wave propagation are

observed. First, the wave breaking point shifts to the seaward direction at $x/h = 2.25$; second, the formation of a moderate standing wave at $x/h = 1.5$ (Fig. 4(b)). These changes occur as the sediments are removed from the seawall toe and more wave energy is reflected from the seawall and the exposed concrete revetment.

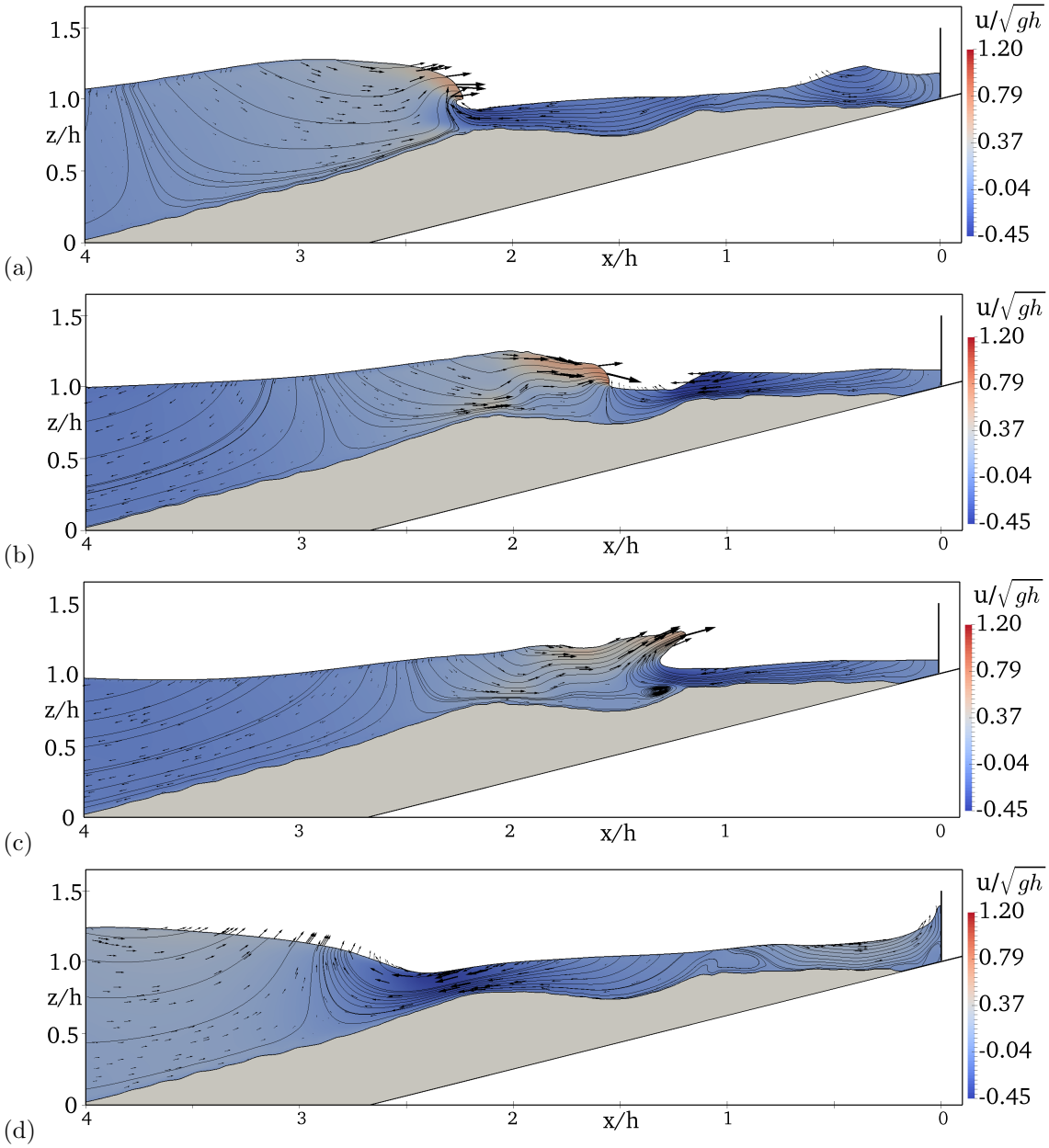

Figure 4: The simulated overturning of wave and impact on the seawall during the intermediate stage of the scouring process at time interval, (a) $t_m/T = 800$, (b) $t_m/T = 800.1$, (c) $t_m/T = 800.3$, (d) $t_m/T = 800.7$

Fig. 5 shows the final stage of the scouring process. The sand berm is seen to be eroding up to $x/h = 0.5$ from the seawall toe and a deep scour hole of about $S/h = 0.25$ is observed at $x/h = 1.5$. Figs. 5(a-b) show the scour at $t_m/T = 1600$ and 1600.1, when the incident wave is breaking at $x/h = 2.5$; the swash is pushed upwards and a reflected wave from the seawall can be seen at $x/h = 0.25$. At this stage, the free surface level, the velocities under the swash and the reflected wave are of similar magnitude but opposite direction. Fig. 5(c) shows the interaction of the swash and the reflected wavefront, leading to an increased wave height. Unlike in the initial stage, the streamlines under the standing wave demonstrate two counter-rotating vortices. This results in a further lift-up mechanism for sediment particles in the scour hole. Fig. 5(d) shows the wave hydrodynamics after the attenuation of the standing wave. Part of the flow is diverted into the offshore direction and mobilises the stirred-up sediments further offshore. The flow diverted to the seawall leads to an impact on the wall and results in the scour at the toe. The water returns in form of a reflected wave and carries the sediments further offshore. Fig. 5(e) shows scour seen after $t_m/T = 1650$ through a comparison between the simulated seabed profile and the experimental observations [4]. The major scour is seen in two places. One scour location is the seawall toe, which is caused by the vertical jet at the seawall. The sediment bed from the seawall toe is found to be eroded until about $x/h = 0.50$. The second large scour is seen at $x/h = 1.5$. It is due to the higher water motion from the interaction of the swash and the reflections from the seawall followed by the formation of a standing wave at this location. The simulated scour profile shows a satisfactory agreement with the experimental data [4].

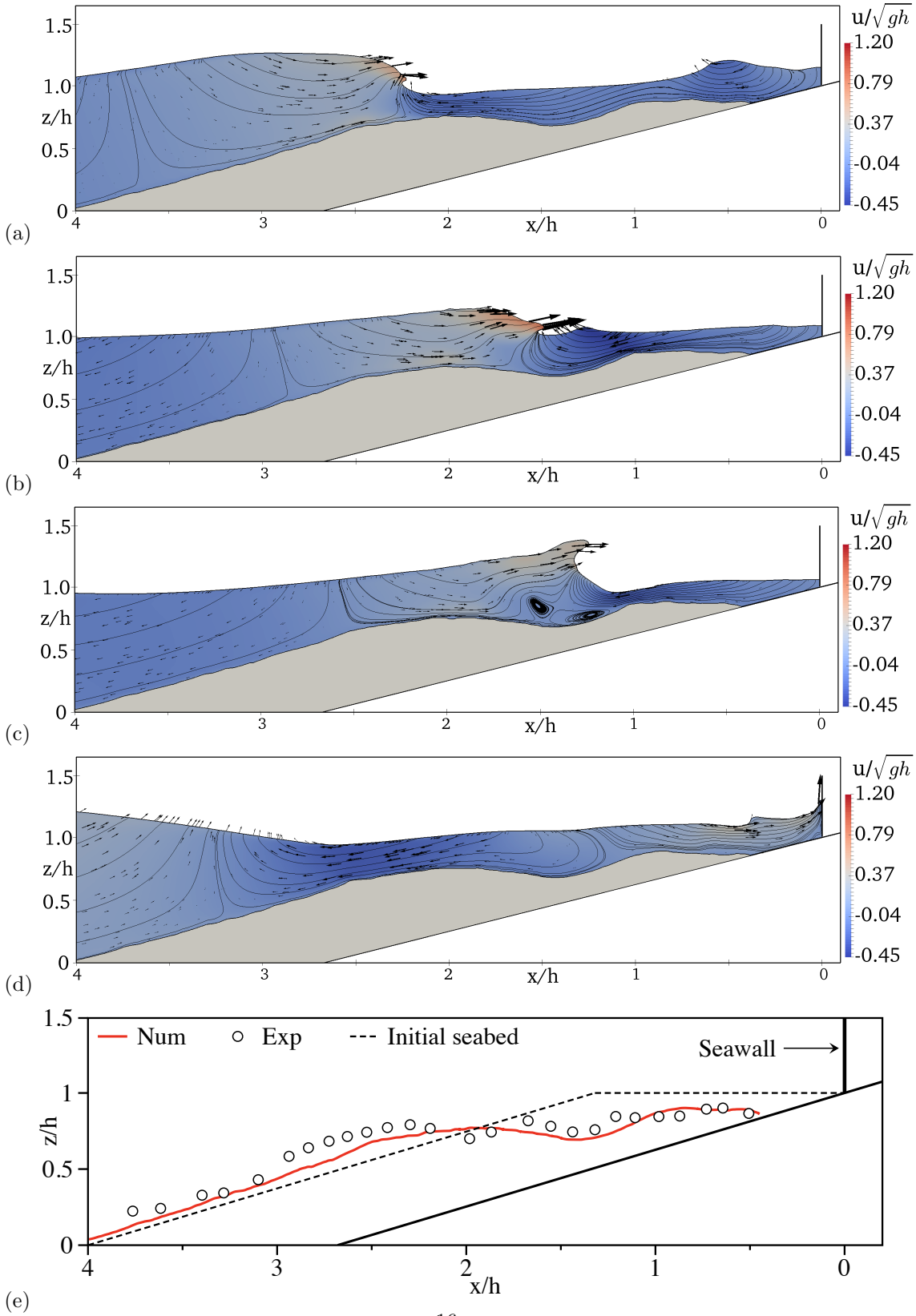

Figure 5: The simulated overturning of wave and impact on the seawall at time interval, (a) $t_m/T = 1600$, (b) $t_m/T = 1600.1$, (c) $t_m/T = 1600.3$, (d) $t_m/T = 1600.7$. (e) simulated scour profile $t_m/T = 1650$. The red line is the simulation and the circles are the experimental data for scour profile. Source of experimental data: Hughes and Fowler [4] (Test T10: regular waves impact on the seawall)

4. Seawall scour for different seawall locations, wave and seabed slope conditions

This section investigates the physics of seawall scour under different scenarios. The numerical setup used for the simulations is the same as used for the validation. Different seawall locations, wave height and seabed slopes are simulated. As the concrete revetment below the sand berm limits the maximum scour depth, it is replaced with a sand berm until the bottom. The other conditions of the simulations, such as the length of the numerical setup, the still water depth, the sediment properties and the simulation duration are similar to the previous simulation of seawall scour.

No	dx	x_w/h	m	h (m)	$T(s)$	H_0 (m)	λ_0 (m)	H_0/λ_0	ξ_0	S/h	S/H_0
Model validation											
B1	0.10	0	1:4	0.67	2.2	0.20	5.5	0.036	1.31	-	-
Effect of the seawall location											
C1	0.10	-0.75	1:4	0.67	2.2	0.20	5.5	0.036	1.31	0.15	0.50
C2	0.10	-0.25	1:4	0.67	2.2	0.20	5.5	0.036	1.31	0.21	0.70
C3	0.10	0.0	1:4	0.67	2.2	0.20	5.5	0.036	1.31	0.30	1.05
C4	0.10	0.25	1:4	0.67	2.2	0.20	5.5	0.036	1.31	0.25	0.83
C5	0.10	0.75	1:4	0.67	2.2	0.20	5.5	0.036	1.31	0.10	0.33
Effect of the wave height											
D1	0.10	0	1:4	0.67	2.2	0.05	5.5	0.009	2.62	0.06	0.80
D2	0.10	0	1:4	0.67	2.2	0.10	5.5	0.018	1.85	0.10	0.67
D3	0.10	0	1:4	0.67	2.2	0.15	5.5	0.027	1.51	0.18	0.80
D4	0.10	0.0	1:4	0.67	2.2	0.20	5.5	0.036	1.31	0.30	1.05
D5	0.10	0	1:4	0.67	2.2	0.25	5.5	0.045	1.17	0.36	0.96
Effect of the seabed slope											
E1	0.10	0	1:2	0.67	2.2	0.20	5.5	0.036	2.62	0.50	1.67
E2	0.10	0	1:4	0.67	2.2	0.20	5.5	0.036	1.31	0.30	1.05
E3	0.10	0	1:6	0.67	2.2	0.20	5.5	0.036	0.87	0.22	0.73
E4	0.10	0	1:8	0.67	2.2	0.20	5.5	0.036	0.66	0.18	0.60
E5	0.10	0	1:10	0.67	2.2	0.20	5.5	0.036	0.52	0.10	0.33

Table 2: A summary of simulations run for seawall scour

The details of the simulations can be found in Table 2. The results show the impact of

the waves at the seawall toe and the resulting scour while computing the complex free surface pattern of breaking and reflected waves.

4.1. Effect of the seawall locations

To illustrate the effect of different seawall locations, five locations x_w/h = -0.75, -0.25, 0, +0.25, +0.75 are discussed. Here $x_w/h = 0$ corresponds to a seawall placed at the intersection between the seabed and the still water level. The negative and positive values of the non-dimensional parameter x_w/h correspond to the seawall located onshore and offshore from the intersection point, respectively. For these simulations, the incident wave height is $H_0 = 0.20$ m, the wave period is $T = 2.2$ s and the bed slope is $m = 1{:}4$ as only the seawall locations are changed.

Fig. 6(a) shows the seabed profile for the seawall placed at x_w/h= -0.75. The wave breaking point is observed between $x/h = 0$ and 0.50. As the seawall is located at about $x/h = 1.25$ from the wave breaking point, the major part of the wave energy is dissipated during the wave run-up before impact on the seawall. Consequently, a reduced wave impact on the seawall can be observed which results in lesser scour (see Fig. 6(f-g) for the value of wave impact at the seawall toe and the corresponding scour depths). The maximum scour depth at the seawall toe is seen to be $S/h = 0.15$ after $t_m/T = 1650$. Fig. 6(b) shows the seawall scour profile when the seawall is placed at x_w/h= -0.25. The maximum scour depth is seen to be $S/h = 0.21$. An increase in the scour depth can be traced back to the close vicinity of the seawall to the surf zone leading the seawall to experience a relatively higher wave impact compared to x_w/h= -0.75. A secondary small scour is seen at $x/h = 2.5$, which is due to the formation of standing waves. Fig. 6(c) shows the scour depth when the seawall is placed at the intersection between the sloping bed and the still water depth, $x_w/h = 0$. The maximum scour at the seawall toe is seen to be $S/h = 0.30$. A further increase in the scour at the seawall toe is caused by the seawall placed nearer to the surf zone, where it experiences a stronger wave impact. Fig. 6(d) shows the scour at the seawall when the seawall is located at $x/h = 0.25$. This case corresponds to a condition when the seawall toe is submerged. The maximum scour depth at the seawall toe is seen to be about $S/h = 0.25$ after $t_m/T = 1650$, which is lower compared to the scour depth seen for $x_w/h = 0$. A decrease in the maximum scour depth indicates less wave energy dissipation as the waves are directly reflected from the seawall.

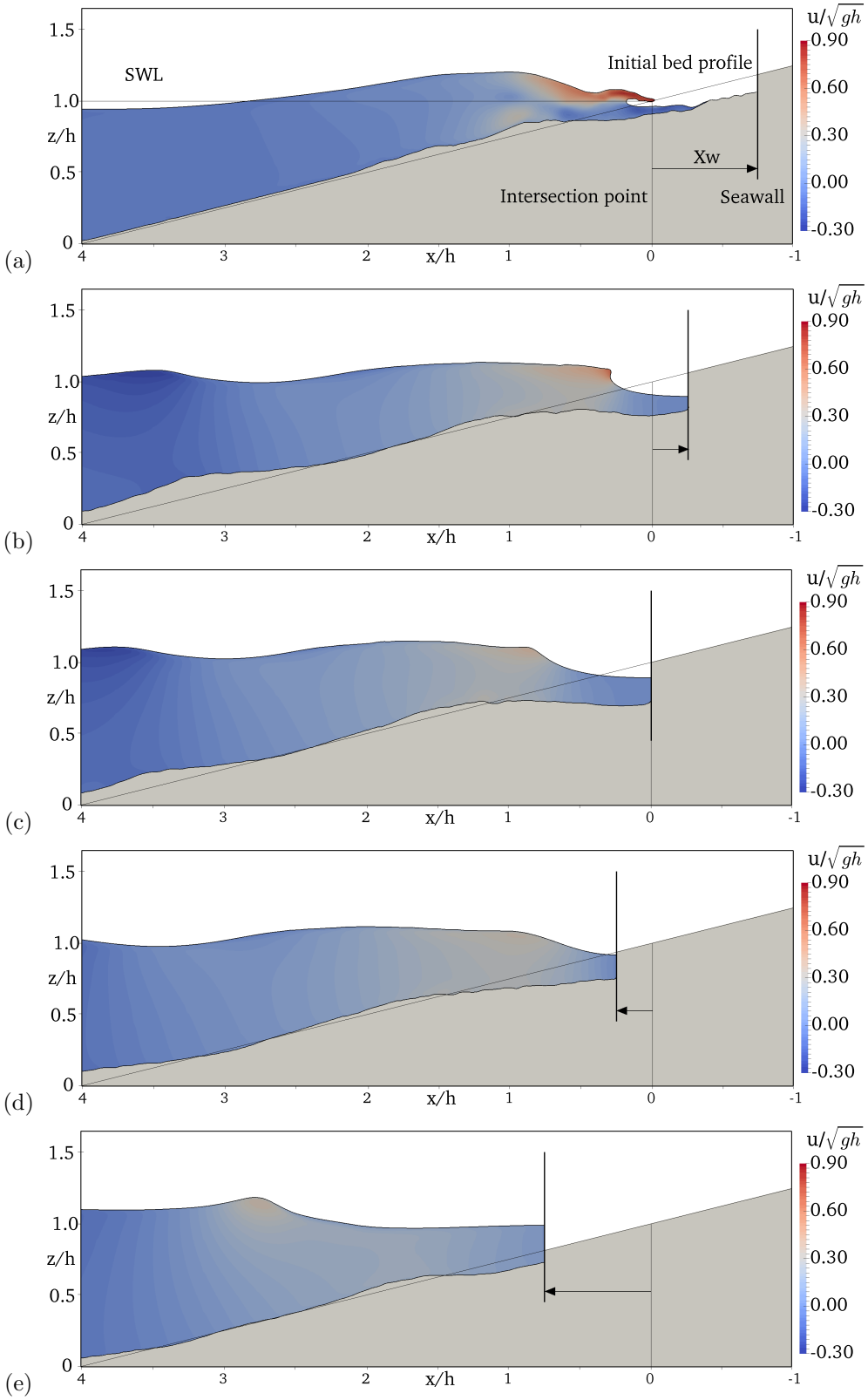
(a)
(b)
(c)
(d)
(e)
SWL
Initial bed profile
Xw
Intersection point
Seawall
z/h
x/h
u/√gh
1.5
1.0
0.5
0
4
3
2
1
0
-1
0.90
0.60
0.30
0.00
-0.30

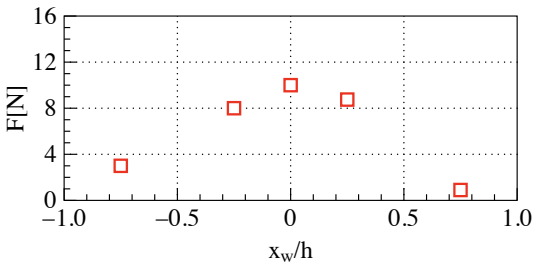

(f) The wave impact at seawall toe corresponding to x_w/h

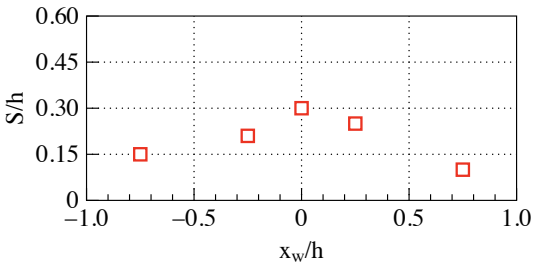

(g) S/h against x_w/h

Figure 6: Seawall scour with free surface profile after $t_m/T = 1650$. The seawall location (a) x_w/h = -0.75, (b) x_w/h = -0.25, (c) $x_w/h = 0$, (d) $x_w/h = 0.25$, (e) $x_w/h = 0.75$. The red squares are the simulated values

In addition, the breaking wave impact and the momentum transfer to the seabed are reduced due to increased water depth at the seawall toe. Overall, the bed shear stress is reduced which results in a smaller scour depth [46]. Fig. 6(e) shows the scour at the seawall when the seawall is located further seawards at $x/h = 0.75$. The maximum scour depth at the seawall is reduced to about $S/h = 0.10$.

Figs. 6(f-g) depict the wave impact experienced at the seawall toe and the resulting scour depth at the seawall toe S/h corresponding to the seawall location x_w/h. The wave impact (F) is calculated by integrating the pressure (p) and shear stress τ over the surface Ω at the seawall toe. The surface normal vectors are produced for the pressure and the shear stress at seawall toe. This can be represented as $\mathbf{F} = \int_\Omega (-\mathbf{n}p + \mathbf{n} \cdot \tau) d\Omega$. The location of the seawall toe can be found in Fig. 1(a). Details of the equation can be found in Kamath et al. [47]. The results indicate that the wave impact is maximum for $x_w/h = 0$ and consequently the maximum scour depth occurs for this case. When the seawall is located away from the intersection point ($x_w/h = 0$) in either direction (onshore or offshore), the wave impact and consequently the scour depth at seawall toe reduces.

4.2. Effect of wave height

In order to illustrate the effect of the wave height on the seawall scour depth, four simulations are run with the incident wave height $H_0 = 0.05$, 0.10, 0.15, 0.20 and 0.25 m. The seawall location is $x_w/h = 0$. The wave period is $T = 2.2$ s and the bed slope is $m = 1{:}4$.

Fig. 7(a-b) shows the scour profile for the incident wave height $H_0 = 0.05$ m and $H_0 = 0.10$ m. A small scour is seen at the seawall toe and the remaining profile is found to be unchanged.

Some deposition can be seen downstream from the eroded area. The scour depth is seen to be $S/h = 0.06$ and 0.10 for $H_0 = 0.10$ m and 0.05 m, respectively. Fig. 7(c) shows the scour profile for $H_0 = 0.15$ m. The maximum scour at the seawall toe is seen to be $S/h = 0.16$ (see Fig. 7(e-f)). The increase in scour depth is attributed to an increase in the wave impact. There is no secondary scour on the sloping bed, which signifies no influence of a standing wave. Fig. 7(d) shows the seabed profile with the free surface for a simulation with the incident wave height $H_0 = 0.25$ m. The maximum scour depth at the seawall toe is seen to be $S/h = 0.36$. The second largest scour is observed at $x/h = 2$ which is due to the formation of a standing wave. The scour depth is higher compared to the other simulations with different values of H_0. This confirms that the wave impact increases with the wave height leading to a higher bed shear stress and consequently to an increased scour depth at the seawall toe. Fig. 7(e-f) presents the variation of wave impact observed at the seawall toe and S/h with the normalised incident wave height H_0/h. The results show that F and S/h increase with H_0/h. The numerical results are compared with the experimental observations [2]. It can be seen that the numerical results for the change in S/h with H_0/h are in good agreement with the measured data [2].

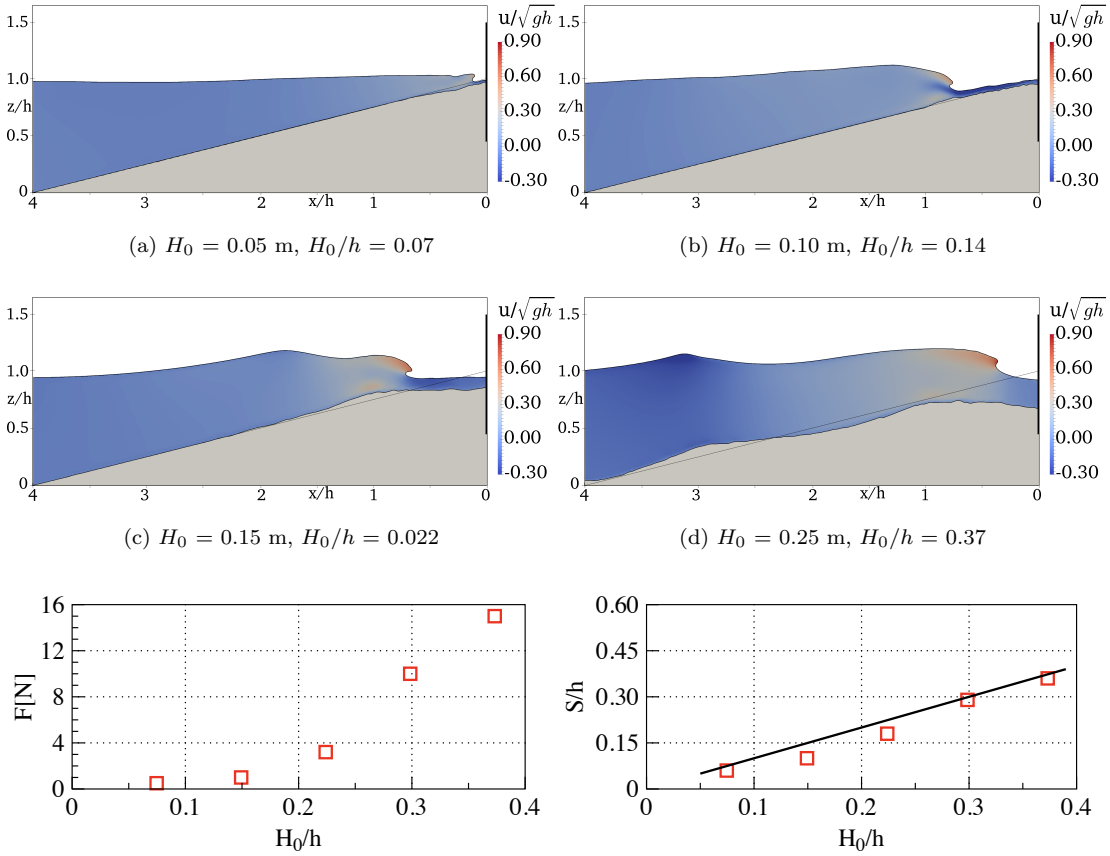

(a) $H_0 = 0.05$ m, $H_0/h = 0.07$

(b) $H_0 = 0.10$ m, $H_0/h = 0.14$

(c) $H_0 = 0.15$ m, $H_0/h = 0.022$

(d) $H_0 = 0.25$ m, $H_0/h = 0.37$

(e) An increase in wave impact F with H_0/h

(f) S/h against H_0/h

Figure 7: The effect of the wave height. (a-d) Seawall scour with free surface profile after $t_m/T = 1650$. (e-f) The red squares are the simulated values and the solid black line is the experimental data from Kraus and McDougal [2]

4.3. Effect of bed slopes

This section describes the variation in the scour depth with changes of the seabed slope (m). Simulations are run for m = 1:10, 1:8, 1:6 and 1:2. Other conditions, such as the incident wave height $H_0 = 0.20$ m, the wave period $T = 2.2$ s and the seawall location $x_w/h = 0$ are maintained. For these simulations, the surf similarity parameter ξ_0 varies between 0.52 and 2.62, which results in plunging breaking waves, as $\xi_0 \geq 0.55$. Figs. 8(a-b) show the seabed profile for the seabed slopes m = 1:10 and 1:8 and the scour is seen be to $S/h = 0.10$ and 0.18, respectively (see Fig. 8(e-f)). The results indicate an increased scour depth with increasing seabed slopes. On milder bed slopes, the waves shoal longer and more wave energy is dissipated in the breaking wave process on the slopes.

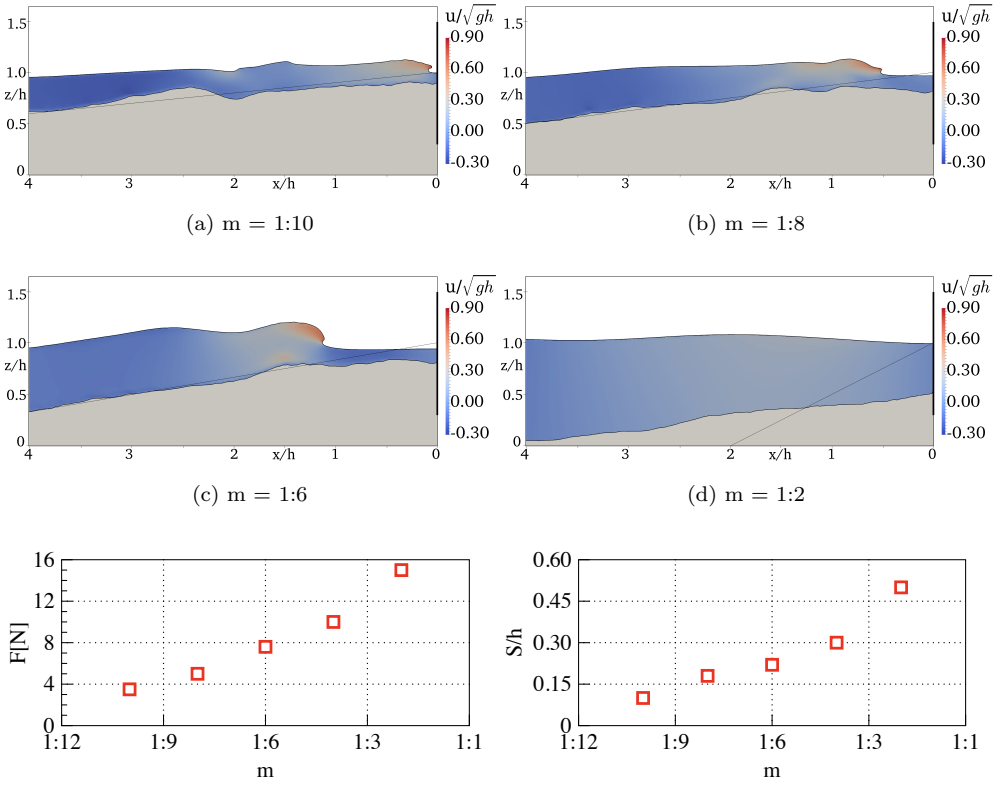

(a) m = 1:10 (b) m = 1:8

(c) m = 1:6 (d) m = 1:2

(e) F versus m (f) S/h against m

Figure 8: Effect of the bed slopes. (a-d) Seawall scour with free surface profile after $t_m/T = 1650$. (e-f) The red squares are the simulated values

Figs. 8(c-d) show the scour profile for the seabed slopes m = 1:6 and 1:2 and the scour is seen to be $S/h = 0.22$ and 0.50, respectively. It can be seen that the steepest slope (m=1:2) results in the maximum scour, with the steeper bed slope the bed shear stress is reduced further (see Eq. 7). Also, the angle of repose is reached quicker, activating the sand slide mechanism with sediments sliding down the slope. Consequently, sediment transport is further accelerated. In this case, breaking takes place later as the shoaling starts relatively late. Then, breaking occurs for larger wave heights with a stronger downward directed jet that increases the bed shear stress. Figs. 8(e-f) depict the wave impact at the seawall toe and the resulting scour for different seabed slopes. An increase in the wave impact and scour at the seawall toe with increasing m is observed.

4.4. Effect of surf similarity parameter ξ_0

Figs. 9(a-b) show the wave impact (F) and the scour depth normalised with the incident wave height (S/H_0) versus the surf similarity parameter (ξ_0). The results are based on the numerical simulations run for seawall scour with incident wave heights between 0.05 m and 0.25 m, and the bed slopes range between m = 1:2 and 1:10 with the wave period T = 2.2 s. The surf similarity parameter ξ_0 range between 0.5 and 3.3, which implies a plunging type breaker. A strong correlation between S/H_0 corresponding to ξ_0 is apparent. The normalised scour at the seawall toe S/H_0 increases from 0.35 to 1 for $0.5 < \xi_0 < 1.3$; reaches to its maximum value of $S/H_0 = 1$, for $\xi_0 = 1.3$; and is then slightly decreasing to $S/H_0 = 0.8$ with a nearly constant value for $1.3 < \xi_0 < 3.3$. The decrease in S/H_0 for $\xi_0 > 1.3$ is due to the change in wave breaking location, wave energy dissipation and consequently the wave impact at the seawall toe (see Fig. 9(a)) which governs the seawall scour.

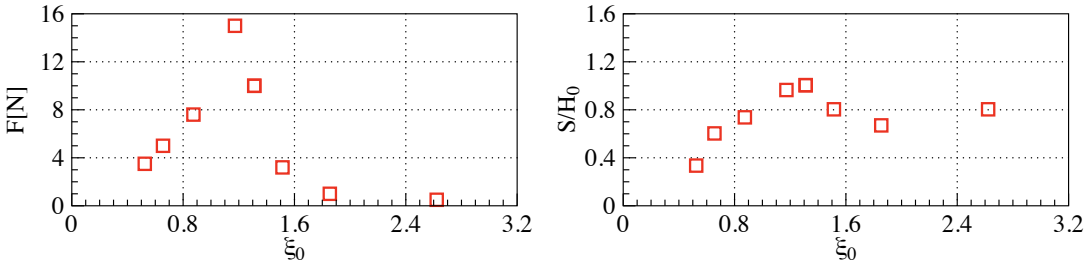

(a) F versus ξ_0 (b) S/H_0 versus ξ_0

Figure 9: Variation of the wave impact at seawall toe and the resulting change in scour depth with the surf similarity parameter ξ_0. In this figure, the value of S/H_0 correspond to the simulations run for seawall located at still water depth and bed slope $m >$ 1:2. The red squares are the simulated values

5. Conclusions

The paper discusses the numerical modelling of scour due to wave impact on a vertical seawall. The modelling of the flow field is based on the solution of the RANS equations and the k-ω turbulence model. The breaking waves and the resulting complex free surface are captured with the level set method. The simulated wave field is coupled with the sediment transport module. The sediment transport module involves calculation of the bed load and suspended load. The effect of the sloping bed on the critical bed shear stress is involved. In order to predict a realistic scour profile, a sand slide algorithm is employed to ensure accurate slope angles inside the scour hole. Bed changes are based on Exner's formula.

The quality of the wave field is ensured through a thorough grid convergence study. The results indicate no influence of the reflected waves from the sloping bed on the wave generation zone and the incident waves approaching the sloping seabed show an adequate agreement with wave theory and the experimental data. The model is then applied to simulate the seawall scour due to the wave impact. The numerical results demonstrate the mechanisms associated with the seawall scour. A close comparison between the numerical results and experiments [4] is obtained. Finally, the validated model is used to simulate different scenarios of seawall location, wave height and seabed slope. Based on the analysis of the results of seawall scour after $t_m/T = 1650$, the following conclusions can be drawn:

- The maximum scour is primarily governed by the breaking wave impact on the seawall. However, in the case of higher waves incident on the seawall, the reflected wave from the seawall leads to a gradual development of a standing wave, which creates another scour hole seawards.

- In the case of the seawall placed at different locations, the maximum wave impact is observed when the wall is positioned at the intersection of the sloping bed and the still water depth. Consequently, the higher scour depth at the seawall toe is observed for this location. A displacement of the wall from the intersection either offshore or onshore direction leads to a decrease in wave impact and consequently a decrease in the scour depth at seawall toe.

- The wave impact and the resulting scour depth is seen to be increasing with the incident wave height (H_0). For the higher waves ($H_0/h > 0.25$), two scour holes are observed. One is due to the wave impact on the seawall and another is due to the formation of a standing wave. The simulated results confirm the experimental observation of $S/H_0 \leq 1.0$ [2].

- The seawall scour increases with increasing seabed slope steepness. For a mild slope, most of the wave energy is dissipated before impact on the seawall. This results in a reduced wave impact and consequently a small scour at the seawall toe. However, for the steep slopes, the incident waves break in front of the wall. Thus, a stronger wave impact and larger scour depth at the seawall toe is observed.

- The seawall scour depth versus the surf similarity parameter shows almost a linear increase in S/H_0 range between 0.35 to 1.0 as ξ_0 increases from 0.5 to 1.3. However, the scour depth is seen to be about $S/H_0 = 0.80$ for $\xi_0 > 1.3$ without any significant change in the

scour depth as ξ_0 increases further.

Acknowledgements

The study has been performed under the POL- NOR/200336/95/2014. The authors are grateful to the Research Council of Norway for this grant. This study has also been supported in part with Sustainable Arctic Marine and Coastal Technology (SAMCoT, WP6) and computational resources at the Norwegian University of Science and Technology (NTNU) provided by NOTUR, http://www.notur.no.

References

[1] S. Vitousek, P. L. Barnard, C. H. Fletcher, N. Frazer, L. Erikson, C. D. Storlazzi, Doubling of coastal flooding frequency within decades due to sea-level rise, Scientific reports 7 (1) (2017) 1399.

[2] N. C. Kraus, W. G. McDougal, The Effects of Seawalls on the Beach: Part I, An Updated Literature Review, Journal of Coastal Research 12 (3) (1996) 691–701.

[3] R. G. Dean, Coastal armoring: effects, principles and mitigation, in: Coastal Engineering 1986, 1843–1857, 1987.

[4] S. A. Hughes, J. E. Fowler, Technical report CERC-90-8: Midscale physical model validation for scour at coastal structures, Tech. Rep., Coastal Engineering Research Center Vicksburg, MS, 1990.

[5] J. E. Fowler, Technical Report CERC-92-16: Scour problems and Method of Prediction of Maximum Scour at Vertical Seawalls, Tech. Rep., Department of the Army, Waterways Experiment Station, Corps of Engineers, Vicsburg, Mississippi U.S., 1992.

[6] J. Kamphuis, K. Rakha, J. Jui, Hydraulic model experiments on seawalls, in: Proceedings 23rd Coastal Engineering conference, ASCE, 1272–1284, 1992.

[7] N. C. Kraus, J. M. Smith, SUPERTANK Laboratory Data Collection Project: Volume I: Main text, Technical report: CERC-94-3 U.S. Army Engineer Waterways Experiment Station, Coastal Engineering Research centre, Vicksburg, MS. .

[8] B. Sumer, J. Fredsøe, Experimental study of 2D scour and its protection at a rubble-mound breakwater, Coastal Engineering 40 (1) (2000) 59–87.

[9] J. Sutherland, C. Obhrai, R. J. S. Whitehouse, A. M. C. Pearce, Laboratory tests of scour at a seawall, in: 3rd International Conference on Scour and Erosion, 3-5 July 2007, Gouda, The Netherlands, 2006.

[10] C. P. Tsai, H. B. Chen, S. S. You, Toe Scour of Seawall on a Steep Seabed by Breaking Waves, Journal of Waterway, Port, Coastal, and Ocean Engineering 135 (2) (2009) 61–68.

[11] W. R. Dally, R. G. Dean, Suspended Sediment Transport and Beach Profile Evolution, Journal of Waterway, Port, Coastal, and Ocean Engineering 110 (1) (1984) 15–33.

[12] J. A. Roelvink, M. J. F. Stive, Bar-generating cross-shore flow mechanisms on a beach, Journal of Geophysical Research: Oceans 94 (C4) (1989) 4785–4800, ISSN 2156-2202.

[13] W. G. McDougal, N. C. Kraus, H. Ajiwibowo, The effects of seawalls on the beach: part II, numerical modeling of SUPERTANK seawall tests, Journal of Coastal Research (1996) 702–713.

[14] K. Gislason, J. Fredsøe, B. M. Sumer, Flow under standing waves: Part 2. Scour and deposition in front of breakwaters, Coastal Engineering 56 (3) (2009) 363 – 370, ISSN 0378-3839.

[15] D. Myrhaug, M. C. Ong, Random wave-induced scour at the trunk section of a breakwater, Coastal Engineering 56 (5-6) (2009) 688–692.

[16] S.-L. Xie, Scouring patterns in front of vertical breakwaters and their influences on the stability of the foundations of the breakwaters, Delft University of Technology, 1981.

[17] Q. Zou, Z. Peng, P. Lin, Effects of wave breaking and beach slope on toe scour in front of a vertical seawall, Coastal Engineering Proceedings 1 (33) (2012) 122, ISSN 2156-1028.

[18] N. Ahmad, H. Bihs, M. Alagan Chella, Ø. A. Arntsen, CFD Modelling of Arctic Coastal Erosion due to Breaking Waves, International Journal of Offshore and Polar Engineering 28 (2018).

[19] M. Alagan Chella, H. Bihs, D. Myrhaug, M. Muskulus, Breaking characteristics and geometric properties of spilling breakers over slopes, Coastal Engineering 95 (2015) 4–19.

[20] M. Alagan Chella, H. Bihs, D. Myrhaug, M. Muskulus, Hydrodynamic characteristics and geometric properties of plunging and spilling breakers over impermeable slopes, Ocean Modelling 103 (2016) 53–72.

[21] H. Bihs, A. Kamath, M. Alagan Chella, A. Aggarwal, Ø. A. Arntsen, A new level set numerical wave tank with improved density interpolation for complex wave hydrodynamics, Computers & Fluids 140 (2016) 191–208.

[22] H. Bihs, A. Kamath, A combined level set/ghost cell immersed boundary representation for floating body simulations, International Journal for Numerical Methods in Fluids 83 (12) (2017) 905–916.

[23] N. Ahmad, H. Bihs, D. Myrhaug, A. Kamath, Ø. A. Arntsen, Three-dimensional numerical modelling of wave-induced scour around piles in a side-by-side arrangement, Coastal Engineering 138 (2018) 132 – 151.

[24] M. S. Afzal, H. Bihs, A. Kamath, Ø. A. Arntsen, Three-Dimensional Numerical Modeling of Pier Scour Under Current and Waves Using Level-Set Method, Journal of Offshore Mechanics and Arctic Engineering 137 (3) (2015) 032001.

[25] D. C. Wilcox, Turbulence modeling for CFD, DCW Industries Inc., La Canada, California., 1994.

[26] S. Osher, J. A. Sethian, Fronts propagating with curvature-dependent speed: algorithms based on Hamilton-Jacobi formulations, Journal of Computational Physics 79 (1988) 12–49.

[27] D. Peng, B. Merriman, S. Osher, H. Zhao, M. Kang, A PDE-based fast local level set method, Journal of Computational Physics 155 (1999) 410–438.

[28] M. Sussman, P. Smereka, S. Osher, A level set approach for computing solutions to incompressible two-phase flow, Journal of Computational Physics 114 (1994) 146–159.

[29] L. C. van Rijn, Sediment Transport, Part I: Bed Load Transport, Journal of Hydraulic Engineering 110 (10) (1984) 1431–1456.

[30] S. Dey, Threshold of sediment motion on combined transverse and longitudinal sloping beds, Journal of Hydraulic Research 41 (4) (2003) 405–415.

[31] H. Bihs, Three-dimensional numerical modeling of local scouring in open channel flow, Report, Department of Hydraulic and Environmental Engineering, Norwegian University of Science and Technology, Trondheim, Norway, 2011.

[32] L. C. van Rijn, Sediment Transport, Part II: Suspended Load Transport, Journal of Hydraulic Engineering 110 (11) (1984) 1613–1641.

[33] J. Hunt, The turbulent transport of suspended sediment in open channels, in: Proceedings of the Royal Society of London A: Mathematical, Physical and Engineering Sciences, vol. 224, The Royal Society, 322–335, 1954.

[34] H. Rouse, Modern conceptions of the mechanics of turbulence, Trans. ASCE 102 (1937) 463–543.

[35] N. R. B. Olsen, Three-Dimensional CFD Modeling of Self-Forming Meandering Channel, Journal of Hydraulic Engineering 129 (5) (2003) 366–372.

[36] M. Burkow, M. Griebel, A full three dimensional numerical simulation of the sediment transport and the scouring at a rectangular obstacle, Computers & Fluids 125 (2016) 1–10.

[37] H. Bihs, N. R. B. Olsen, Numerical modeling of abutment scour with the focus on the incipient motion on sloping beds, Journal of Hydraulic Engineering 137 (10) (2011) 1287–1292.

[38] G. S. Jiang, C. W. Shu, Efficient implementation of weighted ENO schemes, Journal of Computational Physics 126 (1996) 202–228.

[39] C. W. Shu, S. Osher, Efficient implementation of essentially non-oscillatory shock capturing schemes, Journal of Computational Physics 77 (1988) 439–471.

[40] M. Griebel, T. Dornseifer, T. Neunhoeffer, Numerical simulation in fluid dynamics: a practical introduction, SIAM, 1998.

[41] A. Chorin, Numerical solution of the Navier-Stokes equations, Mathematics of Computation 22 (1968) 745–762.

[42] H. van der Vorst, Bi-CGSTAB: A fast and smoothly converging variant of Bi-CG for the solution of nonsymmetric linear systems, SIAM Journal on scientific and Statistical Computing 13 (1992) 631–644.

[43] S. F. Ashby, R. D. Falgout, A parallel multigrid preconditioned conjugate gradient algorithm for groundwater flow simulations, Nuclear Science and Engineering 124 (1) (1996) 145–159.

[44] N. G. Jacobsen, D. R. Fuhrman, J. Fredsøe, A wave generation toolbox for the open-source CFD library: OpenFOAM, International Journal for Numerical Methods in Fluids 70 (9) (2012) 1073–1088.

[45] P. A. Berthelsen, O. M. Faltinsen, A local directional ghost cell approach for incompressible viscous flow problems with irregular boundaries, Journal of Computational Physics 227 (2008) 4354–4397.

[46] A. Roulund, B. M. Sumer, J. Fredsøe, J. Michelsen, Numerical and experimental investigation of flow and scour around a circular pier, Journal of Fluid Mechanics 534 (2005) 351–401.

[47] A. Kamath, M. Alagan Chella, H. Bihs, . A. Arntsen, Evaluating wave forces on groups of three and nine cylinders using a 3D numerical wave tank, Engineering Applications of Computational Fluid Mechanics 9 (1) (2015) 343–354.